Microaspiration for high-pressure freezing: a new method for ultrastructural preservation of fragile and sparse tissues for TEM and electron tomography

W. J. Triffo[1]*, H. Palsdottir[1], K. L. McDonald[1], J. K. Lee[1], J. L. Inman[1], M. J. Bissell[1], R. M. Raphael[1], M. Auer[1]

[1] Departments of Life Sciences, Biophysics, and GTL, Lawrence Berkeley National Laboratory, Berkeley, CA USA

* Corresponding author: W.J. Triffo, Life Sciences Division, Lawrence Berkeley National Laboratory. Address: One Cyclotron Road, Mailstop: Donner, Berkeley CA 94720. Tel: (510) 486-7940, Fax: (510) 486-6488, email: WJTriffo@lbl.gov.

High-pressure freezing is the preferred method to prepare thick biological specimens for ultrastructural studies. However, the advantages obtained by this method often prove unattainable for samples that are difficult to handle during the freezing and substitution protocols. Delicate and sparse samples are difficult to manipulate and maintain intact throughout the sequence of freezing, infiltration, embedding, and final orientation for sectioning and subsequent TEM imaging. An established approach to surmount these difficulties is the use of cellulose microdialysis tubing to transport the sample. With an inner diameter of 200 micrometers, the tubing protects small and fragile samples within the thickness constraints of high-pressure freezing, and the tube ends can be sealed to avoid loss of sample. Importantly, the transparency of the tubing allows optical study of the specimen at different steps in the process. Here, we describe the use of a micromanipulator and microinjection apparatus to handle and position delicate specimens within the tubing. We report two biologically significant examples that

benefit from this approach, 3D cultures of mammary epithelial cells and cochlear outer hair cells. We illustrate the potential for correlative light and electron microscopy as well as electron tomography.

INTRODUCTION

In preparation for ultrastructural analysis by TEM, high-pressure freezing is the preferred method for cryofixation of biological specimens that are thicker than 10 μm, but thinner than 300 μm (Müller & Moor, 1984; Gilkey & Staehelin, 1986; Moor, 1987; Dahl & Staehelin,1989). However, at a practical depth of 100-200 μm, the size limitation imposed by the metal planchette for sample loading may introduce requirements not encountered in more conventional methods that rely on aldehyde fixation protocols. Tissues that are normally handled in larger pieces may become friable when dissected at this size, making it difficult to load the specimen and maintain their integrity throughout processing. Smaller specimens such as single cell suspensions can be spun down to a pellet for easier handling, but centrifugation is undesirable for some specimens due to their delicate nature. Another significant problem in sample preparation is that the specimen may be too sparse to yield a pellet of significant size. Problems associated with loss of small samples and sample fragility propagate through subsequent processing in freeze substitution and resin embedment, which require multiple solution exchanges and manual handling. Further, many experiments, such as those involving correlative light and electron microscopy of the same specimen, require precise tracking and orientation of specific regions within a sample. This information is often difficult to preserve with existing processing methods.

Cellulose microdialysis tubing has proven useful in the preparation of cell suspensions and small samples such as *Caenorhabditis elegans* embryos

(Hohenberg et al., 1994; Müller-Reichert et al., 2003). In addition to facilitating handling during subsequent processing steps, the cellulose tubing has the added benefit of being transparent in the light microscope. Previous implementations of this approach have relied on either capillary action or the use of a pipette to load the sample into the tubing for further processing (Müller-Reichert et al. 2007). The volume enclosed by 1-2 millimeter segments of tubing is well below a microliter; at such small displacements, sparse and/or delicate samples may require a greater degree of precision in specimen manipulation than that provided by previous methods.

Here we describe the use of a micromanipulator and microaspiration setup to allow accurate and predictable positioning of such samples within dialysis tubing. We discuss results from two samples which benefit from this technique: (1) 3D cultures of mouse mammary organoids used as a model system to study breast tissue biology in health and disease (Barcellos-Hoff et al., 1989; Aggeler et al., 1991), and (2) guinea pig outer hair cells (OHCs), which are isolated in a sensory epithelium that is 1-2 cell layers thick and are vital to mammalian hearing (Brownell et al., 1985; Kachar et al., 1986; He et al., 2006; Spector et. al., 2006).

MATERIALS AND METHODS

An overview of this method is illustrated in the flow diagram of Figure 1. Steps that are required for TEM are listed in the right column, while corresponding opportunities for light microscopy for process evaluation or

correlative studies are shown to the left. In addition to the general aspiration approach, details specific to our example specimens are given below.

Micromanipulation and microaspiration

Figure 2 shows the assembled configuration including stereoscope, micromanipulator, and microaspiration system. A Sutter Xenoworks Analog Microinjector (Sutter Inst. Co., CA, USA) with a 100 µL Hamilton syringe was used for aspiration and positioning of specimens within the Spectrapor dialysis tubing (Spectrum Labs, CA, USA). Short segments of tubing were joined to a 1 mm outer diameter glass capillary with 0.5 mm inner diameter using nail polish; this capillary was then mated to the micropipette holder of the microinjector. Mineral oil was used as the hydraulic fluid throughout the system up to the junction with the capillary. A Siskiyou MX110 4-axis manual micromanipulator (Siskiyou, Inc., OR, USA) attached to a magnetic base was used for fine positioning of the cellulose tubing.

Making and using the crimping tool

A well-crafted tool for crimping the microdialysis tubing is essential for success (Müller-Reichert et al. 2007). The tip was cut off of a number 11 scalpel blade, leaving a blunt edge about 1mm in width. Using a whetstone or grinding wheel, the tip was shaped to have a double bevel of about 45 degrees from each side (Fig. 2b-c). The burr on the cutting edge was removed by a few strokes on a fine whetstone. It is important to avoid making the cutting edge too sharp or it will

just cut the tubing and not crimp it. While cutting, tubing was always submerged in a fluid such as 20% bovine serum albumin (BSA, w/v) or 1-hexadecene to avoid rapid drying out of the specimen. We preferred to cut in a polypropylene plastic petri dish due to its compliance, though other plastics may work as well. A simple rocking motion in the direction parallel to the cutting edge sufficed to cut and crimp the tubing. To test the crimping ability of the blades, microdialysis tubing was loaded with a dye such as toluidine blue and cut in 1-hexadecene.

Preparation of samples

a. Mouse organoids

The procedure to isolate and culture primary mouse mammary gland epithelial organoids in 3D has been described in detail previously (Simian et al., 2001). Prior to design of the microaspirator we tried growing the organoids inside the cellulose tubes in order to best maintain the integrity of extracellular matrix material. We plated the mammary organoids in Matrigel in wells containing sterilized segments of the tubing. However, by growing the organoids inside the tubes, their number and density could not be easily adjusted, leading to sparsely populated tubes (data not shown). The resulting low density of organoids in tubes is not practical for labor intense, high throughput optical pre-screening of the typically heterogeneous 3D cultures to select suitable candidates for subsequent ultrastructural analysis. Also, diffusion of high molecular weight components from the growth media, such as transferrin (ca. 80 kDa) and prolactin (ca. 24 kDa), is restricted to the open ends of the 1 mm length of tube, as the tubes have a

molecular weight cut-off of 13-18 kDa. As a solution to this problem, a suspension of mouse mammary organoids grown in Matrigel was prepared for aspiration using the method described here.

Organoids were grown for 10 days inside Matrigel (BD Biosciences, Bedford, MA, USA) in DMEM/F12 supplemented with insulin/ transferrin/sodium selenite (Sigma), and penicillin/streptomycin (UCSF Cell Culture Facility, San Francisco, USA). Functional differentiation was induced by addition of the lactogenic hormones prolactin (3 μ g/mL; Sigma) and hydrocortisone (1 μ g/mL; Sigma) to the cell culture media. The organoids in Matrigel were rinsed with 1mL of cold PBS-EDTA with a protease inhibitor cocktail (Calbiochem, San Diego, CA, USA) and pipetted with a wide bore pipette to gently tease the Matrigel apart. The solution was transferred to a 15mL conical tube on ice and shaken for 1.5 hours on ice at 4°C. The organoids were gently spun at 1000 rpm for 10 minutes at 4°C and then resuspended in PBS for microaspiration.

b. Guinea pig outer hair cells

Hartley albino guinea pigs were anesthetized by isofluorane and decapitated with a guillotine. The temporal bones were removed and the organ of Corti was exposed by dissection in Invitrogen Medium 199 containing Hanks' salts (Invitrogen Corp., CA, USA). Strips of the sensory epithelium were transferred using a 200 µL pipette and placed in a 35 mm MatTek dish (MatTek Corp, MA, USA); enzymatic digestion was avoided to preserve long strips of

tissue. Strips containing OHCs were then identified by stereoscope and selected for further manipulating/handling using the microaspirator.

Loading specimens into the microdialysis tubing

Using the device in Figure 2, samples were selected under magnification from their original buffer, transferred to cryoprotectant if desired, and then re-aspirated. Once the sample was positioned in the tube, the distal end of the tube was closed using the crimping tool. The proximal end was then cut free and crimped.

For a dialysis tube with an inner diameter of 200 μm, a 1 mm long segment will enclose a volume of approximately 30-35 nL. With a displacement of 100 nL per full turn of the fine control knob, we found that a 100 μL Hamilton syringe provided adequate precision for positioning of the sample within the tube. In spatial resolution, the Siskiyou MX110 micromanipulator gives a precision of approximately 10 μm for each independent axis. This level of control proved invaluable for selecting and manipulating specific samples from dilute solutions, along with maximizing occupied space in the tubing during the crimping process. Sample exchanges from native buffer to cryoprotectant were also done on each individual sample using the device. This controlled the time of specimen exposure to the cryoprotectant, and also allowed for tracking of the sample prior to freezing.

High-pressure freezing and freeze substitution (HPF/FS)

Prior to freezing, the tubes are cut and crimped to 1 –1.5 mm lengths so that they fit into the aluminum hats used as freezing platforms. A filler material is added to prevent trapped air around the specimen. It is also important that this filler serve as a cryoprotectant, providing good heat conduction and discouraging the formation of crystalline ice. Non-penetrating fillers with low osmotic activity, such as gelatin, BSA, and dextran, are recommended, but in some cases we have used 10% glycerol successfully, especially when working with aldehyde pre-fixed specimens. Glycerol has the advantage of serving as a cryoprotectant with lower viscosity than BSA and dextran fillers, but it should be noted that possible artifacts associated with using glycerol are well documented (Gilkey and Staehelin, 1986). Aware of the pitfalls, we have used 10% glycerol as a filler in structural studies of cell junctions that have cytoskeletal attachments in prefixed biological material where potential extraction of cytoplasm and membrane artifacts are not detrimental to the object of interest.

Specimens were aspirated into tubes in cryoprotectant made with either 10% glycerol (v/v) or 20% BSA (w/v) in their original buffer. Tubes were placed in 200 μm deep aluminum planchettes, the remaining space in the planchette was filled with cryoprotectant, and the specimens were cryo-immobilized using a BAL-TEC HPM-010 high-pressure freezer (BAL-TEC, Inc., Carlsbad, CA; Müller & Moor, 1984; Gilkey & Staehelin, 1986; Moor, 1987; Dahl & Staehelin, 1989). Samples were then freeze-substituted in 1% osmium tetroxide and 0.1% uranyl acetate in acetone using a Leica AFS (Leica Microsystems, Vienna, Austria) following a previously described protocol (McDonald, 2007). In some samples, 1-

2% water was added to enhance membrane contrast (Walther and Ziegler, 2002). Following freeze substitution, specimens were washed with several rinses of pure acetone before being infiltrated in either Durcupan ACM (Electron Microscopy Sciences, PA, USA) or an Epon-Araldite mixture (McDonald & Müller-Reichert, 2002). The tubes were flat-embedded between two slides using two layers of parafilm as a spacer (Müller-Reichert et al., 2003).

Staining tubes with safranin-O

Microdialysis tubing can be difficult to see during the infiltration and embedding solution changes. To prevent sample loss during specimen processing we experimented with cellulose binding dyes on cryo-immobilized and freeze-substituted tubes. Histologic stains for cellulose are one way to visualize the transparent tubes, aiding in detection of the specimen during acetone dehydration and graded series of resin exchanges. The cationic stain safranin-O appears brilliant red in the lignified cellulose of plant cell walls. Accordingly, we successfully employed safranin-O (Gurr, 1971), staining the tubes bright red when added in trace amounts (a couple of grains per ml) during acetone rinses before resin embedding. In cases where the high-pressure freezing filler is cross-linked during freeze substitution, e.g. with dextran or BSA, it is not necessary to color the tubes because the entire contents of the freezing planchette can be treated as one piece.

Light microscopy for sample processing

For loading and manipulation of cellulose tubing prior to freezing, an Olympus SZX12 stereoscope was used (Olympus America, Inc., PA, USA) with epi- and trans-illumination provided by a pair of Fostec 150W lamps (Olympus). Flat embedded specimens were also screened using the SZX12, which provided up to 144x effective zoom. After orientation and mounting, 500 nm thick sections were cut and stained with toluidine blue.

Staining for light microscopy

Immunofluorescence was performed on organoids isolated from Matrigel. Samples were fixed in 50:50 methanol:acetone for 10 min at -20°C. Samples were blocked in PBS + 5% goat serum + 1:100 dilution of F(ab)2 (Jackson Lab, Bar Harbor, USA) for one hour. Samples were then incubated in a FITC-conjugated ZO-1 antibody (Zymed, USA) that recognizes the tight junction protein ZO-1 at 1:100 dilution overnight at 4°C. Samples were washed and stained for nuclei with Hoechst 33258 and imaged using epifluorescence on a Zeiss Axiovert 200 inverted microscope (Carl Zeiss Microimaging, Inc., NY, USA). OHCs in tubes were fixed in 4% paraformaldehyde in PBS, permeabilized in 0.1% Triton X-100 in PBS, stained for actin with Alexa Fluor 555 phalloidin (Invitrogen), and subsequently imaged using a Zeiss LSM 410 confocal microscope (Zeiss). Figure 3a-b shows mouse organoids visualized before cryofixation with phase contrast optical microscopy (Fig. 3a) and indirect visualization of ZO-1 using fluorescence (Fig. 3b). Figure 3 c-d shows low and

high magnification views of mouse organoids embedded in Epon-Araldite resin in the cellulose tubing prior to sectioning and transmission electron microscopy.

Transmission electron microscopy

70-100 nm thin sections were collected on formvar coated slot grids and post-stained with 2% uranyl acetate in 70% methanol followed by either Reynold's or Sato's lead citrate (Sato, 1968). Sections were imaged on either an FEI Tecnai 12 TEM (FEI, Eindhoven, Netherlands) on Kodak 4489 film or a Phillips CM200 TEM (FEI) with a Tietz TemCam-F214 CCD camera (TVIPS GmbH, Martinsried, Germany). Images were processed using ImageJ (Abramoff et al., 2004).

Electron tomography

Tilt series of 150 nm sections were collected at 1° increments through a range of +/- 70° using EMMENU 3.0 software (TVIPS) on a Phillips CM200 TEM (FEI) equipped with a Fischione Advanced Tomography Holder (E. A. Fischione Instruments, Inc., PA, USA) and a Tietz TEMCam-F214 CCD camera (TVIPS). Series were aligned with 5 nm gold fiducials and reconstructed using the IMOD software package (Kremer et al., 1996). Post-processing and segmentation of the resulting volume density maps was done using a combination of IMOD and the UCSF Chimera package (Pettersen et al., 2004).

RESULTS AND DISCUSSION

Mammary epithelial 3D cultures

Primary cultures of mouse mammary epithelial cells or organoids retain their tissue-specific functions when grown in laminin-rich extracellular matrix (lrECM) gel. Here we grew mouse mammary organoids in Matrigel, a laminin-rich basement membrane gel produced by the Engelbreth-Holm-Swarm murine tumor (Kleinman et al., 1986). These 3D cultures retain the functional features of the mouse mammary gland *in vivo* and even synthesize milk proteins when induced by addition of lactogenic hormones (Barcellos-Hoff et al., 1989; Aggeler et al., 1991).

Upon high-pressure freezing and freeze substitution the mouse mammary organoids show excellent preservation, as can be seen in Figures 4a-f. The organoids are composed of an outer layer of myoepithelial cells (Fig. 4b: MyEp) and an inner layer of epithelial cells that enclose a lumen (Fig. 4b: LuEp). Secretory activity is manifest by numerous secretory granules - presumably vesicles with milk proteins - along with lipid inclusions that are round, smooth, free of ice crystal formation, and devoid of infiltration artifacts (Figure 4c). Notably, the materials secreted into the lumen are not aggregated, but instead appear as a homogeneous distribution of density as expected for well-preserved specimens. The lumen is sealed by tight junctions, shown in Fig. 4d. As previously documented by ultrastructural evaluation of 3D cultured mammary epithelia by conventional means, the nuclear profile is irregular with numerous cytoplasmic invaginations (Barcellos-Hoff et al., 1989; Underwood et al., 2006).

The nuclear architecture is well preserved, clearly showing nucleoli and nuclear pores, and discrimination of densely stained heterochromatin from less dense DNA is possible (Fig 4c, Fig. 4e). Tissue specific differentiation of the organoids is evident in the increase of well-developed rough endoplasmatic reticulum corresponding to the lactogenic hormone-induced production of milk protein and fatty acids (Fig. 4f).

It is now widely appreciated that simulation of the physiological 3D microenvironment in cell cultures is essential to the maintenance of cellular function and meaningful conclusions from in vitro model systems. This requirement has been shown extensively in the study of both rodent and human cell lines that model many aspects of the mammary gland and breast cancer (Bissell et al., 2005). As illustrated here, when evaluating phenotypically crucial features of 3D cell cultures such as epithelial microvilli formation and cell junction architecture, ultrastructure remains a critical tool not currently replaceable by optical methods.

As evident from the electron micrographs, this preparation protocol and subsequent cryo-immobilization does not disrupt the acinar architecture of the organoids (Fig. 4a-b). Even the intrinsic basal lamina that is secreted by the organoid upon cultivation in lrECM is intact and attached by hemidesmosomes to the isolated organoid (Fig. 4b). We propose this method of microaspiration prior to cryo-immobilization for high-throughput ultrastructural evaluation of organoids. In fact, this method is practical for handling any type of isolated 3D cultures that are fragile and difficult to detect by eye during processing.

Outer hair cells

For this material the use of microdialysis tubing and the micromanipulator alleviated several barriers during sample preparation, which had proved intractable by other methods. The objective was faithful preservation of the OHC lateral wall by HPF/FS, which includes both internal membrane and cytoskeletal components within 50 nm of the lateral plasma membrane. Because of the inevitable variability in cell health within the dissected epithelium and osmotic sensitivity of the OHCs, it was necessary to test large populations of OHCs under a variety of conditions. The ability to observe and evaluate each sample from the dissecting dish, through the freezing and substitution process, and during flat embedment for orientation, allowed the efficient screening of large numbers of OHCs in each experiment to select the best preserved cells for subsequent ultrastructural and electron tomographic analysis. OHCs are under turgor pressure and exquisitely sensitive to changes in osmolarity (Chertoff et al. 1994). When using a 10% v/v solution of glycerol in buffer as a cryo-protectant, the effective osmolarity of the solution often resulted in the collapse of the extracisternal space (ECS) lying between the plasma membrane and the closely approximated lamellae, known as the subsurface cisternae (data not shown). Using the microaspirator, we were able to systematically screen a variety of cryo-protectants; Figure 5 shows results obtained using 20% w/v bovine serum albumin (BSA), which has much lower effective osmolarity than glycerol. The

cytoplasm of the OHC ECS is intact rather than collapsed, and its associated cytoskeletal components are well preserved.

The lack of internal membrane contrast frequently observed in freeze-substituted samples was also a problem with the subsurface cisternae (SSC). Variation of the freeze substitution medium such as the addition of water (Walther & Ziegler, 2002) resulted in improved SSC contrast compared to the standard medium; we found that 2% water gave sufficient contrast for our studies. The tomography results shown in panels d-f of Figure 5 illustrate the fidelity that we were able to achieve by varying cryo-protectant and freeze-substitution parameters. To our knowledge, this is the first successful preservation of the main features of the OHC lateral wall (SSC and the cytoskeletal components of the ECS) by high-pressure freezing and freeze substitution.

Application of microaspiration and microdialysis tubing in correlative light and electron microscopy studies

An exciting prospect in modern microscopy is the ability to correlate results from light microscopy and TEM on the same high-pressure frozen specimen (Biel et al., 2003; Pelletier et al., 2006; Müller-Reichert et al., 2007). The ability to preserve both recombinant and synthetic fluorophores through high-pressure freezing, freeze substitution, and resin embedment (Luby-Phelps et. al., 2003; Biel et. al., 2003; Hardie et. al., 2004; Krisp et al., 2006) along with development of photo-conversion techniques (Gaietta et al., 2002; Grabenbauer

et al., 2005) broadens this potential to augment pre-existing live cell fluorescence studies with direct ultrastructural correlation. Further extension from 2D to 3D data is available through the use of confocal LM at sub-micrometer resolution, and TEM tomography at nanometer resolution (Frey et al., 2006). Microaspiration into cellulose dialysis tubing provides a unique route to facilitate tracking of specific samples among different imaging modalities. To illustrate this potential, the panel in Figure 5 proceeds through a series of figures in progressively smaller scale, from a low-magnification 2D overview of an entire embedded tube containing an OHC strip at approximately 10 μm resolution to a 3D electron tomogram of the OHC lateral wall that based on objective criteria (Cardone et al., 2005) displays a resolution of 3-4 nm (Triffo et al., manuscript in preparation). For many samples, this method will provide a reliable route to bridging this resolution gap under controlled, identical specimen treatment.

Other useful applications and advantages

Another important feature of the dialysis tubing is its permeability to low molecular weight solutes, which allowed us to carry out all steps “in-tube” for the fluorescence labeling sequence that led to the confocal image of Figure 5b, from Triton X-100 permeabilization to labeling with AlexaFluor555-phalloidin. The permeability of the dialysis tubing should also allow “in-tube physiology” studies, where pharmacologic stimuli meeting this size requirement could be applied and be effective on the specimen up until the commencement of freezing. This would be a particularly interesting application for transient stimuli whose effects may be

subtle in magnitude and begin to dissipate immediately upon removal. As an example application which we are pursuing, acetylcholine, a neurotransmitter that modulates OHC motility and is believed in part to affect cytoskeletal remodeling (Frolenkov, 2006), can be applied just prior to freezing, allowing ultrastructural analysis without aldehyde fixation. Such studies would be difficult to carry out for unprotected samples, as trauma during mechanical handling may cause artifacts that would confound the effects of the pharmacological agent.

Because this aspiration approach permits the use of dilute specimens, we were able to avoid procedures such as high-speed centrifugation into a dense solution or pellet, which was undesirable for our samples. Along with providing protection for the sample, the tubing increased the effective size of the specimens, making it easier to track the specimen during processing. This also resulted in minimal material loss when considering all steps in the process, from initial selection prior to freezing up through flat embedding in resin.

Summary

The improved resolution and insight provided by electron tomographic 3D reconstruction of cells and tissues and its correlation to optical studies, combined with cryo-immobilization during sample preparation, provides an added dimension to cellular electron microscopy (Frey et al., 2006). As cell biologists delve deeper into the molecular processes driving life by both identifying the individual players and their relational networks, the ability to correlate fluorescence microscopy and ultrastructural *in-situ* 3D analysis of molecular

machines at molecular resolution will become increasingly important. We believe that our microaspiration approach can contribute to this important goal.

ACKNOWLEDGEMENTS

We thank Reena Zalpuri of the UC Berkeley Electron Microscopy Laboratory for her assistance in various aspects of this work. K. L. McDonald wishes to thank Andres Kaech of BAL-TEC company for suggestions on how to make crimping tools, and Jennifer Lonsdale for suggesting safranin-O as a method to color small, clear objects during freeze substitution. Work by W. J. Triffo on this project was supported in part by a DOE CSGF fellowship administered by the Krell Institute, grant DE-FG02-97ER25308, and also supported by an NSF CAREER Award (BES 044379) to R. M. Raphael. This project was supported by National Institutes of Health grant DC07680, and by the Director, Office of Science, of the U.S. Department of Energy under contract DE-AC02-05CH11231 to M. Auer, and in part by OBER, Office of USDOE and NCI grant 5 RO1 CA64786-07 to M. J. Bissell. Correspondence should be directed to W. Jeff Triffo or Dr. Manfred Auer, Department of Biophysics and GTL, Lawrence Berkeley National Laboratory, 1 Cyclotron Road, Berkeley, CA 94720. WJTriffo@lbl.gov, triffo@rice.edu or MAuer@lbl.gov

FIGURE LEGEND

Figure 1. Flow diagram of the generalized protocol. Optional light microscopy (LM) steps are highlighted in gray.

Figure 2. Overview of micromanipulator and microaspiration setup. a. The micromanipulator is at left (red arrow), and microinjector used for aspiration at right (red arrowhead). Flexible hydraulic tubing joins the Hamilton syringe of the injector to the micropipette holder attached to the manipulator. Inset depicts close-up of the region in the red box, illustrating the cellulose tubing (white arrow) mounted to the glass capillary (white arrowhead) held by the micropipette holder of the microinjector. **b-c.** Side **(b)** and top-down **(c)** views of the crimping tool fashioned from a scalpel blade, showing the 45° bevel at the tip.

Figure 3. Microaspiration of mouse organoids isolated from Matrigel 3D cultures. a. Phase contrast optical microscopy of mouse organoid grown in Matrigel. **b**. Fluorescence imaging of immunostaining for ZO-1 (green) and nuclear DAPI (blue) in mouse organoids. **c**. Resin embedded organoids in crimped tube, and **d**. close up of organoids in tube. Scale bars: **(a)** 10 μm; **(b)** 25 μm; **(c)** 200 μm; and **(d)** 50 μm.

Figure 4. Ultrastructural evaluation of mouse mammary organoid grown in 3D Matrigel cultures. a. Overview of the organoid and close up in **b.** showing the two cell types: the luminal epithelial (LuEp) cells embraced by myoepithelial

cells (MyEp). Lumen is annotated Lu. Arrowhead indicates basement membrane. **c**. Vesicles and lipid inclusions (V) are round and well preserved in cryofixed organoids. Nuclear (N) morphology is well preserved and in this view two nucleoli are shown (Nu). **d**. Tight junctions (arrowhead) form a seal around the lumen (Lu). Also shown is an adjacent adherens junction (arrow). Microvilli are depicted (Mv). Mitochondria (asterisk) and intracellular vesicles are well preserved. **e**. and **f**. Concomitant with induced milk protein expression in hormone induced 3D cultures of organoids, the rough endoplasmatic reticulum is prominent (arrowheads). Scale bars: **(a)** 10 µm; **(b)** 2 µm; **(c,e-f)** 1 µm; **(d)** 500 nm.

Figure 5. Multiscale imaging of OHCs. a. Low magnification overview of organ of Corti strip containing OHCs in tube after HPF/FS and flat embedding. **b.** An optical section from an LSM confocal stack shows three intact rows of OHCs using AlexaFluor555-phalloidin to stain actin. **c.** A TEM image of an axial cross-section from the middle of an OHC; arrowheads indicate mitochondria. The orientation of the section is indicated by the dashed line in the inset cartoon of the cylindrical OHC at top right, with apical hair bundle (HB) and nucleus (N) depicted. Dark staining outside the cell is the BSA used as filler and cryo-protectant; the nucleus is at the basal pole of this cell, and thus not seen in this micrograph. **d-f.** Tomography of the region indicated by the box in **(c)**. In the projection image **(d)** and selected mid-tomogram slice **(e)**, the adjacent cell has been masked out in gray for clarity. Arrowheads in **(e)** indicate individual ribosomes; internal membranes are clearly visible along with cytoskeletal detail.

In **(f)**, the plasma membrane (PM, red) and first two cisterns of SSC (blue and yellow) are rendered on top of a single slice from the tomogram, showing the curvature and continuity of the SSC in relation to the PM. Scale bars: **(a)** 200 μm; **(b)** 50 μm; **(c)** 2 μm; **(d-f)** 100 nm.

REFERENCES

Abramoff, M.D., Magelhaes P.J. & Ram, S.J. (2001) Image Processing with ImageJ. Biophotonics International 11 (7): 36-42.

Aggeler, J., Ward, J., Blackie, L.M., Barcellos-Hoff, M.H., Streuli, C.H. & Bissell M.J. (1991) Cytodifferentiation of mouse mammary epithelial cells cultured on a reconstituted basement membrane reveals striking similarities to development in vivo. J Cell Sci. 99: 407-417.

Barcellos-Hoff, M.H., Aggeler, J., Ram, T.G. & Bissell, M.J. (1989) Functional differentiation and alveolar morphogenesis of primary mammary cultures on reconstituted basement membrane. Development 105: 223-235.

Biel, S.S., Kawaschinski, K., Wittem, K.P., Hintze, U. & Wepf, R. (2003) From tissue to cellular ultrastructure: closing the gap between micro- and nanostructural imaging. J. Microsc. 212(Pt 1): 91-99.

Bissell, M.J., Kenny, P.A. & Radisky, D.C. (2005) Microenvironmental regulators of tissue structure and function also regulate tumor induction and progression: the role of extracellular matrix and its degrading enzymes. Cold Spring Harb Symp Quant Biol. 70: 1-14.

Brownell W.E., Bader C.R., Bertrand D. & de Ribaupierre Y. (1985) Evoked mechanical responses of isolated cochlear outer hair cells. Science. 227(4683): 194-196.

Cardone G., Grunewald, K. & Steven, A.C. (2005) A resolution criterion for electron tomography based on cross-validation. J. Struct. Biol. 151(2): 117-129.

Chertoff, M.E. & Brownell, W.E. (1994) Characterization of cochlear outer hair cell turgor. Am. J. Physiol. 266 (2 Pt 1): C467-479.

Dahl, R. & Staehelin, L.A. (1989) High-pressure freezing for the preservation of biological structure: Theory and practice, J. Electron Microsc. Tech. 13: 165-174.

Frey, T.G., Perkins, G.A. & Ellisman, M.H. (2006) Electron tomography of membrane-bound cellular organelles. Annu. Rev. Biophys. Biomol. Struct. 35: 199-224.

Frolenkov, G.I. (2006) Regulation of electromotility in the cochlear outer hair cell. J. Physiol. 1:576(Pt 1): 43-48.

Gaietta, G., Deerinck, T.J., Adams, S.R., Bouwer, J., Tour, O., Laird, D.W., Sosinsky, G.E., Tsien, R.Y. & Ellisman, M.H. (2002) Multicolor and electron microscopic imaging of connexin trafficking. Science. 296: 503-507.

Gilkey, J.C. & Staehelin, L.A. (1986) Advances in ultrarapid freezing for the preservation of cellular ultrastructure. J. Electron Microsc. Techn. 3: 177–210.

Grabenbauer, M., Geerts, W.J., Fernadez-Rodriguez, J., Hoenger, A., Koster, A.J. & Nilsson, T. (2005) Correlative microscopy and electron tomography of GFP through photooxidation. Nat. Methods. 2: 857-862.

Gurr, E. (1971) Synthetic Dyes in Biology, Medicine and Chemistry. Academic Press, London, England.

Hardie, N.A., MacDonald, G. & Rubel, E.W. (2004) A new method for imaging and 3D reconstruction of mammalian cochlea by fluorescent confocal microscopy. Brain Res. 1000: 200-210.

He, D.Z., Zheng, J., Kalinec, F., Kakehata, S. & Santos-Sacchi, J. (2006) Tuning in to the amazing outer hair cell: membrane wizardry with a twist and shout. J. Membr. Biol. 209: 119-134.

Hohenberg, H., Mannweiler, K. & Müller, M. (1994) High-pressure freezing of cell suspensions in cellulose capillary tubes. Journal of Microscopy (Oxford) 175: 34-43.

Kachar, B., Brownell, W. E., Altschuler, R. & Fex, J. (1986) Electrokinetic shape changes of cochlear outer hair cells. Nature. 322: 365-368.

Kremer, J.R., Mastronarde, D.N. & McIntosh, J.R. (1996) Computer visualization of three-dimensional image data using IMOD J. Struct. Biol. 116: 71-76.

Kleinman, H.K., McGarvey, M.L., Hassell, J.R., Star, V.L., Cannon, F.B., Laurie, G.W. & Martin, G.R. (1986) Basement membrane complexes with biological activities. Biochemistry. 25: 312–318.

Krisp, H., von Wichert, G., Seufferlein, T. & Walther, P. (2006) Application of a new High-Pressure Freezing Apparatus. Microsc. Microanal. 12(Supp 2).

Luby-Phelps, K., Ning, G., Fogarty, J. & Besharse, J.C. (2003) Visualization of identified GFP-expressing cells by light and electron microscopy. J. Histoch. Cytoch. 51:271-274.

McDonald, K. (2007) Cryopreparation methods for electron microscopy of selected model systems. Meth. Cell Biol. 79:23-56.

McDonald, K. & Müller-Reichert, T. (2002) Cryomethods for Thin Section Electron Microscopy. In, Guide to Yeast Genetics and Molecular and Cell

Biology, Parts B and C (C. Guthrie and G.R. Fink, eds.), 351, Meth. Enzymol., Academic Press, San Diego, USA, pp. 96-123.

Moor H. (1987) Theory and practice of high-pressure freezing. In: Cryo-techniques in Biological Electron Microscopy, 175-191, ed. By Steinbrecht R. A., Zierold K., Springer Verlag.

Müller, M. & Moor, H. (1984) Cryofixation of thick specimens by high-pressure freezing. In: The Science of Biological Specimen Preparation, Revel, J.P., Barnard T., Haggis G. H. (Eds.) Proc. of the 2nd Pfefferkorn Conference, SEM, Inc. AMF O'Hare, IL, USA. Pp. 131-138.

Müller-Reichert, T., O'Toole, E.T., Hohenberg, H. & McDonald, K.L. (2003) Cryoimmobilization and three-dimensional visualization of C. elegans ultrastructure. J. Microscopy 212: 71-80.

Müller-Reichert, T., Srayko, M., Hyman, T., O'Toole, E. & McDonald, K.L. (2007) Correlative light and electron microscopy of early C. elegans embryos in mitosis. Meth. Cell Biol. 79: 101-119.

Pelletier, L., O'Toole, E., Schawger, A., Hyman, A.A., Müller-Reichert. T. (2006) Centriole assembly in Caenorhabditis elegans. Nature 444: 619-623.

Pettersen, E.F., Goddard, T.D., Huang, C.C., Couch, G.S., Greenblatt, D.M., Meng, E.C. & Ferrin, T.E. (2004) UCSF Chimera - A Visualization System for Exploratory Research and Analysis. J. Comput. Chem. 25: 1605-1612.

Sato, T. (1968) A modified method for lead staining of thin sections. J Electron Microsc (Tokyo) 17: 158-159.

Simian, M., Hirai, Y., Navre, M., Werb, Z., Lochter, A. & Bissell, M.J. (2001) The interplay of matrix metalloproteinases, morphogens and growth factors is necessary for branching of mammary epithelial cells. Development. 128: 3117-3131.

Spector, A.A., Deo, N., Grosh, K., Ratnanather, J.T. & Raphael R.M. (2006) Electromechanical models of the outer hair cell composite membrane. J. Membr. Biol. 209: 135-152.

Underwood, J.M., Imbalzano, K.M., Weaver, V.M., Fischer, A.H., Imbalzano, A.N. & Nickerson, J.A. (2006) The ultrastructure of MCF-10A acini. J Cell Physiol. 208: 141-148.

Walther, P. & Ziegler, A. (2002) Freeze substitution of high-pressure frozen samples: the visibility of biological membranes is improved when the substitution medium contains water. J. Microsc. 208: 3–10.

Figure 1

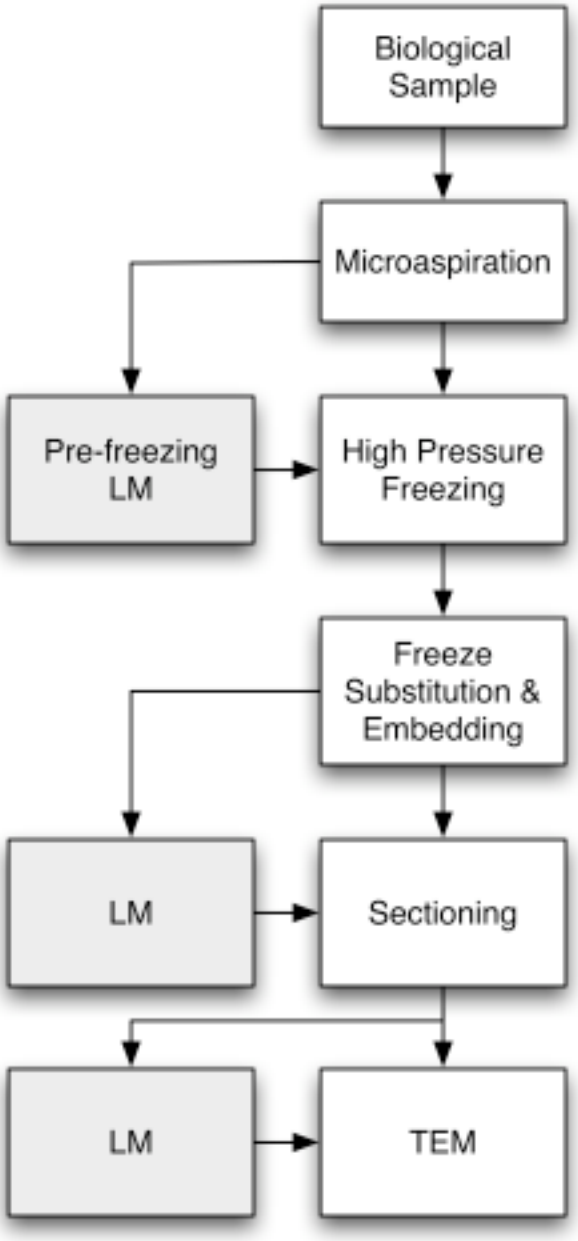
Biological Sample
Microaspiration
Pre-freezing LM
High Pressure Freezing
Freeze Substitution & Embedding
LM
Sectioning
LM
TEM

Figure 2

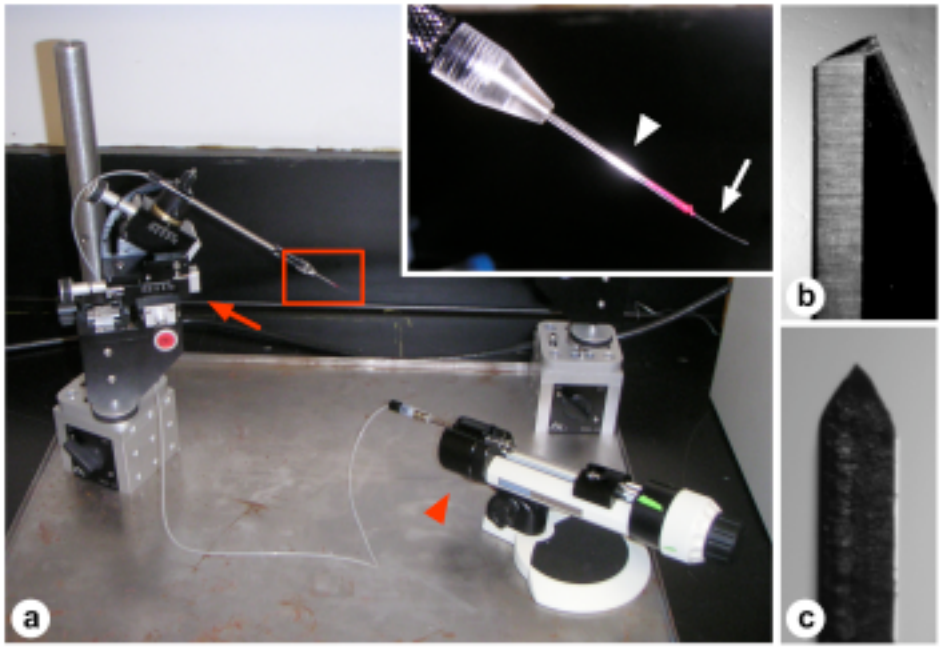

Figure 3

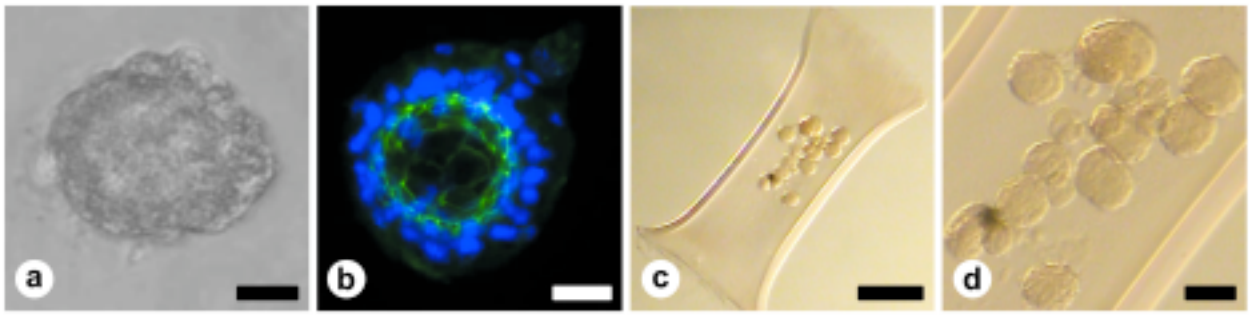

Figure 4

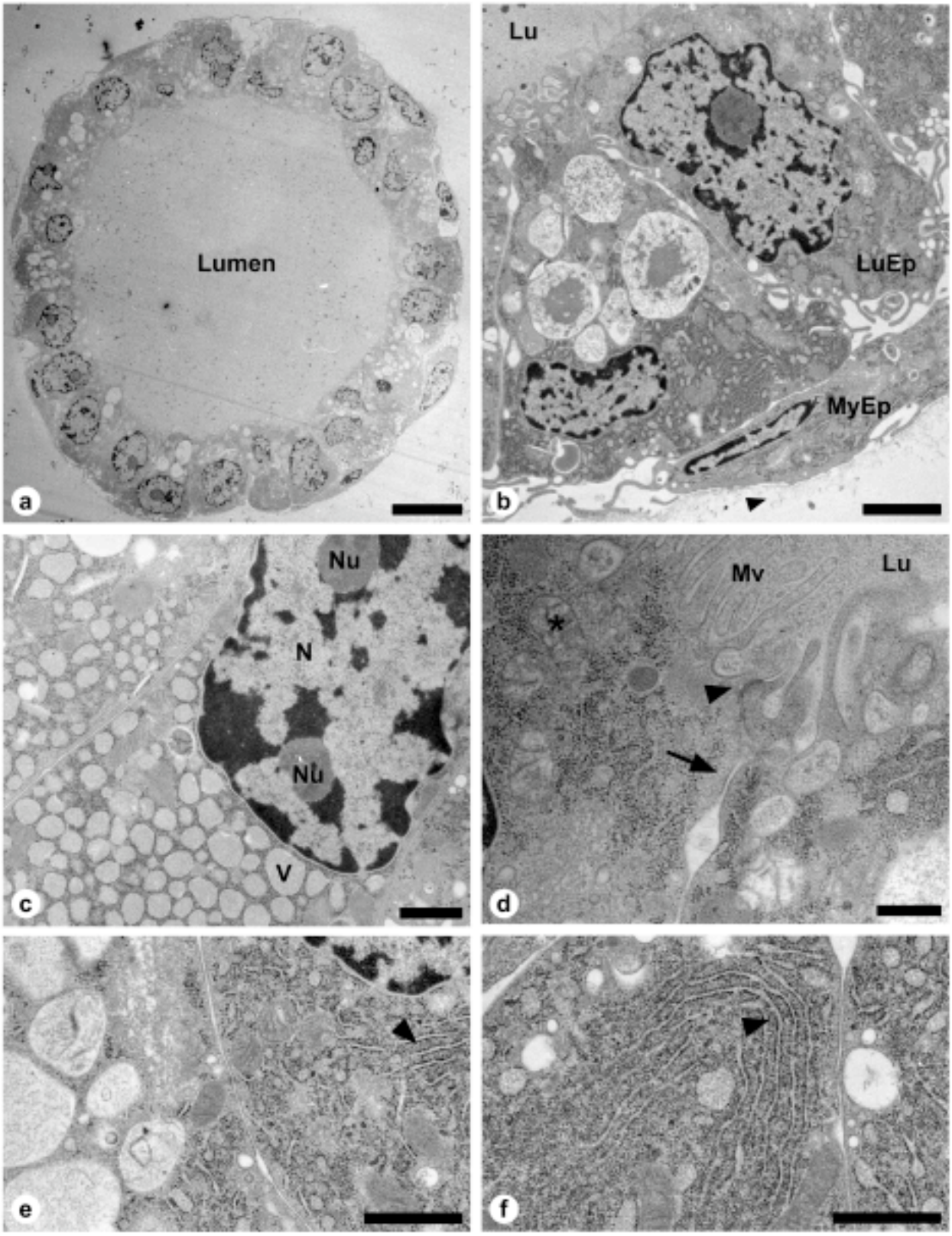

Figure 5